REPORT DOCUMENTATION PAGE

Form Approved OMB NO. 0704-0188

The public reporting burden for this collection of information is estimated to average 1 hour per response, including the time for reviewing instructions, searching existing data sources, gathering and maintaining the data needed, and completing and reviewing the collection of information. Send comments regarding this burden estimate or any other aspect of this collection of information, including suggesstions for reducing this burden, to Washington Headquarters Services, Directorate for Information Operations and Reports, 1215 Jefferson Davis Highway, Suite 1204, Arlington VA, 22202-4302. Respondents should be aware that notwithstanding any other provision of law, no person shall be subject to any oenalty for failing to comply with a collection of information if it does not display a currently valid OMB control number.
PLEASE DO NOT RETURN YOUR FORM TO THE ABOVE ADDRESS.

1. REPORT DATE (DD-MM-YYYY)	2. REPORT TYPE	3. DATES COVERED (From - To)
17-04-2008	Final Report	1-Aug-2004 - 31-Jul-2007

4. TITLE AND SUBTITLE	5a. CONTRACT NUMBER
Development of improved microwave dielectric materials and devices using advanced experimental and theoretical methods	W911NF-04-1-0376
	5b. GRANT NUMBER
	5c. PROGRAM ELEMENT NUMBER
	611102

6. AUTHORS	5d. PROJECT NUMBER
Nathan Newman, Van Schilfgaarde	
	5e. TASK NUMBER
	5f. WORK UNIT NUMBER

7. PERFORMING ORGANIZATION NAMES AND ADDRESSES	8. PERFORMING ORGANIZATION REPORT NUMBER
Arizona State University 31.00 Office of Research & Sponsored Projects Administration Arizona State University Tempe, AZ 85287 -3503	

9. SPONSORING/MONITORING AGENCY NAME(S) AND ADDRESS(ES)	10. SPONSOR/MONITOR'S ACRONYM(S)
U.S. Army Research Office P.O. Box 12211 Research Triangle Park, NC 27709-2211	ARO
	11. SPONSOR/MONITOR'S REPORT NUMBER(S)
	46228-MS.1

12. DISTRIBUTION AVAILIBILITY STATEMENT

Distribution authorized to U.S. Government Agencies Only, Contains Proprietary information

13. SUPPLEMENTARY NOTES

The views, opinions and/or findings contained in this report are those of the author(s) and should not contrued as an official Department of the Army position, policy or decision, unless so designated by other documentation.

14. ABSTRACT

Our work has made important progress towards developing a fundamental understanding of the microscopic mechanism that causes loss in high performance microwave dielectrics, and can explain why some dielectric materials exhibit markedly better performance than others. Ab-initio electronic structure calculations elucidated the physical reason for this desirable microwave properties in Ba(Cd1/3Ta2/3)O3 (BCT) and Ba(Zn1/3Ta2/3)O3 (BZT). The presence of significant charge transfer between cation d-orbitals provides a degree of covalent directional bonding between atoms that resist angular distortions, a property absent in conventional ionic compounds. We have also been able to show a direct correlation between the number

15. SUBJECT TERMS

microwave dielectrics, high-Q, ceramics

16. SECURITY CLASSIFICATION OF:			17. LIMITATION OF ABSTRACT	15. NUMBER OF PAGES	19a. NAME OF RESPONSIBLE PERSON
a. REPORT	b. ABSTRACT	c. THIS PAGE	SAR		Nathaniel Newman
U	U	U			19b. TELEPHONE NUMBER
					480-727-6934

Standard Form 298 (Rev 8/98)
Prescribed by ANSI Std. Z39.18

Report Title

Development of improved microwave dielectric materials and devices using advanced experimental and theoretical methods

ABSTRACT

Our work has made important progress towards developing a fundamental understanding of the microscopic mechanism that causes loss in high performance microwave dielectrics, and can explain why some dielectric materials exhibit markedly better performance than others. Ab-initio electronic structure calculations elucidated the physical reason for this desirable microwave properties in Ba(Cd1/3Ta2/3)O3 (BCT) and Ba(Zn1/3Ta2/3)O3 (BZT). The presence of significant charge transfer between cation d-orbitals provides a degree of covalent directional bonding between atoms that resist angular distortions, a property absent in conventional ionic compounds. We have also been able to show a direct correlation between the number of point defects present and enhanced microwave loss. High quality single-crystalline BZT films were also produced, for the first time. The availability of single crystal materials is essential to the fundamental studies. Zn-enriched targets and high oxygen pressures are used to compensate for Zn loss during film growth. The Ba(Zn1/3Ta2/3)O3 films have an indirect band gap of ~3.0 eV and a refractive index of 1.91 in the visible. Development of high dielectric-constant material with diminished microwave loss and a near-zero temperature coefficient of resonant frequency, will enable the production of smaller and higher performance microwave devices.

List of papers submitted or published that acknowledge ARO support during this reporting period. List the papers, including journal references, in the following categories:

(a) Papers published in peer-reviewed journals (N/A for none)

1) 113.   Structural, chemical and dielectric properties of ceramic injection molded Ba(Zn1/3Ta2/3)O3 microwave dielectric ceramics, Shaojun Liu, Vincent Merrick and N. Newman, J. Europ. Ceram. Soc. 26, 3273 (2006).
2) Structural, Dielectric and Optical Properties of Ni-doped Barium Cadmium Tantalate Ceramics, Hongxue Liu, Shaojun Liu, Victor Y. Zenou, Cameron Beach, and N. Newman, Jap. J. Appl. Phys. 45, 9140 (2006).

Number of Papers published in peer-reviewed journals: 2.00

(b) Papers published in non-peer-reviewed journals or in conference proceedings (N/A for none)

Number of Papers published in non peer-reviewed journals: 0.00

(c) Presentations

1) "Development and optimization of essential tools for the design of electromagnetic band gap filters", Semiconductor Research Corporation Packaging and Interconnect Summer Review, U.C.L.A., Los Angeles, California, July 23, 2007.
2) "Realization of electromagnetic Band Gap Filters using advanced ceramic injection molding methods", Semiconductor Research Corporation Packaging and Interconnect Summer Review, Stanford University, Stanford, California, August 23, 2006.
3) "Investigation of the influence of point defects and microstructure on the high field properties of practical ferroelectric materials", ONR Capacitor Review, San Diego, CA, March 6, 2006.
4) "Development and optimization of essential tools for the design of electromagnetic Band Gap Filters", Semiconductor Research Corporation Packaging and Interconnect Summer Review, Stanford University, Stanford, California, August 25, 2005.
5) "Investigation of the influence of point defects and microstructure on the high field properties of practical ferroelectric materials", ONR Capacitor Review, Arlington, VA, June 10th, 2005.

Number of Presentations: 5.00

Non Peer-Reviewed Conference Proceeding publications (other than abstracts):

Number of Non Peer-Reviewed Conference Proceeding publications (other than abstracts):   0

Peer-Reviewed Conference Proceeding publications (other than abstracts):

Number of Peer-Reviewed Conference Proceeding publications (other than abstracts):   0

(d) Manuscripts

1) Growth and characterization of epitaxial Ba(Zn1/3Ta2/3)O3 (100) thin films, Z.Z. Tang, S.J. Liu, R. K. Singh, S. Bandyopadhyay, I. Sus, M van Schilfgaarde and N. Newman, submitted to Journal of Applied Physics.

2) Influence of point defects induced by neutron irradiation on the microwave dielectric properties of Ni and Zr-doped Ba(Zn1/3Ta2/3)O3 ceramics, Shaojun Liu, H. X Liu, and N. Newman, submitted to Applied Physics Letters.

Number of Manuscripts: 2.00

Number of Inventions:

Graduate Students

NAME	PERCENT SUPPORTED
Zhizhong Tang	0.80
Shaojun Liu (until 2005)	0.10
Hongxue Liu	0.20
Inna Suss	0.40
FTE Equivalent:	**1.50**
Total Number:	**4**

Names of Post Doctorates

NAME	PERCENT SUPPORTED
Shaojun Liu (after 1/06)	0.10
Hongxue Liu	0.10
FTE Equivalent:	**0.20**
Total Number:	**2**

Names of Faculty Supported

NAME	PERCENT_SUPPORTED	National Academy Member
Nathan Newman	0.10	No
Mark van Schilfgaarde	0.05	No
FTE Equivalent:	**0.15**	
Total Number:	**2**	

Names of Under Graduate students supported

NAME	PERCENT SUPPORTED
Cameron Beach	0.15
Jason Dykert	0.10
FTE Equivalent:	**0.25**
Total Number:	**2**

Student Metrics

This section only applies to graduating undergraduates supported by this agreement in this reporting period

The number of undergraduates funded by this agreement who graduated during this period: 1.00

The number of undergraduates funded by this agreement who graduated during this period with a degree in science, mathematics, engineering, or technology fields:...... 1.00

The number of undergraduates funded by your agreement who graduated during this period and will continue to pursue a graduate or Ph.D. degree in science, mathematics, engineering, or technology fields:...... 1.00

Number of graduating undergraduates who achieved a 3.5 GPA to 4.0 (4.0 max scale): 1.00

Number of graduating undergraduates funded by a DoD funded Center of Excellence grant for Education, Research and Engineering: 0.00

The number of undergraduates funded by your agreement who graduated during this period and intend to work for the Department of Defense 0.00

The number of undergraduates funded by your agreement who graduated during this period and will receive scholarships or fellowships for further studies in science, mathematics, engineering or technology fields: 1.00

Names of Personnel receiving masters degrees

NAME

Total Number:

Names of personnel receiving PHDs

NAME
Shaojun Liu
Hongxue Liu

Total Number: **2**

Names of other research staff

NAME	PERCENT_SUPPORTED	
Rakesh Singh	0.05	No
FTE Equivalent:	**0.05**	
Total Number:	**1**	

Sub Contractors (DD882)

Inventions (DD882)

Development of improved microwave dielectric materials and devices
using advanced experimental and theoretical methods

Final Report

Submitted To: Dr. William Lampert,
US Army Research Office
PO Box 12211
Research Triangle Park, NC 27709-2211
LampertWV@aro.arl.army.mil
Phone: 919-549-4325

P.I.:   Prof. Nathan Newman and Prof. Mark van Schilfgaarde,
School of Materials, ASU, Tempe, AZ 85287-6006.
Ph: 480 727-6934(NN); 965-4977(MvS); FAX: 480 965-0037;
Nathan.Newman@asu.edu; Mark.vanSchilfgaarde@asu.edu

Contract: W911NF0410376

Table of contents:

I. Statement of the problem studied:

Development of high dielectric-constant (ε) material with diminished microwave loss (tan δ) and a near-zero temperature coefficient of resonant frequency (τ_F), will enable the production of smaller and higher performance microwave devices that operate over a wider range of frequencies. *Our work has made important progress towards developing a fundamental understanding of the microscopic mechanism that causes loss in dielectric materials, and can explain why some dielectric materials exhibit markedly better microwave performance than others. We have also been able to show a direct correlation between the number of point defects present and enhanced microwave loss.*

II. List of figures and tables.

Figure 1. Electronic band structure calculated using the LMTO method for $Ba(Zn_{1/3}Ta_{2/3})O_3$ and $Ba(Cd_{1/3}Ta_{2/3})O_3$.

Fig. 2. Rietveld analysis of X-ray diffraction spectra of 0.1 wt% Ni-doped $Ba(Cd_{1/3}Ta_{2/3})O_3$ samples.

Fig. 3 The results of optical measurements in the visible range for $Ba(Zn_{1/3}Ta_{2/3})O_3$ samples with a wide range of Ni and Zr doping. Note the enhanced background signal for material with diminished quality factors (Qs).

Fig. 4 Visible absorption spectra of $Ba(Cd_{1/3}Ta_{2/3})O_3$ samples doped with varying concentrations of Ni.

Figure 5 The magnitude of the observed paramagnetic moment of the Ni and Zr-doped Ba(Zn$_{1/3}$Ta$_{2/3}$)O$_3$ samples as a function of irradiation dose.

Figure 6 Effect of irradiation damage on the dielectric properties of Ni and Zr-doped Ba(Zn$_{1/3}$Ta$_{2/3}$)O$_3$:

Figure 7. Densities-of-states of the four kinds of vacancies in BZT, compared to DOS of bulk BZT (top). The DOS were aligned to the core levels; the Fermi level is shown as a dashed blue line.

Figure 8. Left: Densities-of-states of the Frenkel defects in BZT, compared to DOS of bulk BZT (top). The DOS were aligned to the core levels; the Fermi level is shown as a dashed blue line. Right DOS of the V_{Ba} +V_O Schottky defect.

Figure 9. DOS of Zr: and Ni: doped BZT.

Figure 10(a). Elemental composition in as-grown films fabricated using a stoichiometric Ba(Zn1/3Ta2/3)O3 target; (b)X-ray diffraction data of the same films grown over a range of substrate temperatures.

Figure 11. X-ray diffraction data of the Ba(Zn$_{1/3}$Ta$_{2/3}$)O$_3$ films grown at different substrate temperatures from a Zn-enriched target, and their corresponding compositions as inferred by RBS analysis.

Figure 12. (a-e) Optical characterization of Ba(Zn$_{1/3}$Ta$_{2/3}$)O$_3$ thin film, ceramics and bulk polycrystalline material.

Figure 13. Transmission spectrum of Ba(Zn$_{1/3}$Ta$_{2/3}$)O$_3$ films grown at a 600 °C substrate temperature using a Zn-enriched target

Figure 14 Room temperature dielectric constant and dissipation factor of Ba(Zn$_{1/3}$Ta$_{2/3}$)O$_3$ film, inferred from measurements on interdigital structures. The film was grown from Zn-enriched target at 600 °C substrate temperature

Figure 15. The temperature-dependence of the capacitance and dissipation factor of thin-film Ba(Zn$_{1/3}$Ta$_{2/3}$)O$_3$ interdigital capacitors. The results shown here are for a film grown at a 600 °C substrate temperature from an Zn-enriched target.

Figure 16. The influence of bias on the capacitance and dissipation factor of Ba(Zn$_{1/3}$Ta$_{2/3}$)O$_3$ interdigital capacitors.

Figure 17. The leakage current of Ba(Zn$_{1/3}$Ta$_{2/3}$)O$_3$ thin films measured using an interdigital structure.

Figure 18. The Arrhenius plot of leakage current in the Ba(Zn$_{1/3}$Ta$_{2/3}$)O$_3$ thin films grown from Zn-enriched target at 600 °C substrate temperature.

Table I. Lattice parameters of Ni-doped Ba(Cd$_{1/3}$Ta$_{2/3}$)O$_3$ samples for the cubic and hexagonal structures inferred from Rietveld analysis.

Table II. Atomic Wyckoff positions of Ba(Cd$_{1/3}$Ta$_{2/3}$)O$_3$ in space group *P*-3*m*1 inferred from Rietveld analysis.

III. Summary of the most important results
1. List of key findings

- $Ba(Cd_{1/3}Ta_{2/3})O_3$ (BCT) and $Ba(Zn_{1/3}Ta_{2/3})O_3$ (BZT) fall in the general class of perovskites with the general formula $Ba(B'_{1/3}B''_{2/3})O_3$ (where B' is a divalent metal such as Mg, Zn or Cd and B'' is a pentavalent transition metal such as Ta or Nb). A number of these compounds exhibit the unusual combination of a large dielectric constant and a small tan δ at microwave frequencies. **Our recent work using ab-initio electronic structure calculations elucidated the physical reason for this desirable microwave properties in BCT and BZT.** *The presence of significant charge transfer between the cation d-orbitals provides a degree of covalent directional bonding between atoms that resist angular distortions, a property absent in conventional ionic compounds.* The angular rigidity strengthens "soft lattice modes" and results in higher melting points, enhanced phonon energies and reduced microwave loss. This is critical to achieving low loss in the large Z materials that characteristically have large dielectric constants. In the BCT and BZT cases, charge is transferred from Ta $5d$-levels at and near the conduction band minimum to Cd $-4d$ and Zn $-3d$ levels at and near the VBM.

- *A correlation was found between the loss tangent of Ni-doped BZT and BCT ceramics with the intensity of the continuous absorption background in the optical spectra. This results from the presence of optically active point defects and indicates that point defects play an important role in the microwave loss in BZT and BCT.*

- *A correlation was found between the number of paramagnetic defects produced by particle irradiation of Ni and Zr-doped $Ba(Zn_{1/3}Ta_{2/3})O_3$ samples and the microwave loss.* This again illustrates the role of point defects in degrading microwave performance in practical ceramics.

- *High quality single-crystalline BZT films were produced using Pulsed Laser Deposition.* To our knowledge, this is the first time single crystal thin films of high-performance microwave material have been synthesized. *The availability of single crystal materials is essential to the fundamental studies. Zn-enriched targets and high oxygen pressures are used to compensate for Zn loss during film growth. The $Ba(Zn_{1/3}Ta_{2/3})O_3$ films have an indirect optical band gap of ~3.0 eV and a refractive index of 1.91 in the visible spectral range. A dielectric constant of 25 and dissipation factor of 0.0025 at 100 kHZ has been measured using the interdigital capacitor method. The $Ba(Zn_{1/3}Ta_{2/3})O_3$ films exhibit a small thermally-activated Ohmic leakage current at high fields (<500 KV/cm) and high temperatures (<200 °C) with an activation energy of 0.85 eV.*

- Initial theoretical calculations predict that the relative contribution of d-electron bonding will be stronger in Cd-containing compounds than in the other compounds, including BZT. An important difference that was predicted for BCT is a distortion that results in a bond angle of 172° for the Ta-O-Cd bond. Our recent X-ray diffraction measurements using advanced Reitvild method to analyze the data determined an angle of 173°, very near to the LDA theoretical prediction. This was an *extremely important finding as it confirmed the applicability of local density functional calculations for these highly correlated systems.*

2. Introduction

Dielectric resonators and filters have become increasingly important to the expanding microwave communication market. Originally used in small quantities for high-performance military and civilian satellite applications, their use in cellular telephone systems and global positioning has resulted in a tremendous surge in the quantity commercially manufactured. If significant improvements in the microwave properties of these dielectrics could be realized, it will undoubtedly revolutionize satellite and cellular communication technology.

The microwave performance of devices depends on three important materials parameters: ε (the dielectric constant), ***tan*** $\boldsymbol{\delta}$ (the loss tangent) and τ_F, (temperature coefficient of resonant frequency). For practical applications, high dielectric constant (***ε***) materials are generally preferred to minimize the device dimensions as they typically scales as $\varepsilon^{-1/2}$. For high-Q high-performance devices, materials with low loss (i.e. small ***tan*** $\boldsymbol{\delta}$) are essential. Even though dielectric loss often limits the system performance of a wide range of systems including those used in cellular and satellite communication technology, a basic understanding of the mechanism responsible for this material property has not been firmly established. To minimize the susceptibility of devices to temperature-induced shifts in the operating frequency and to minimize 1/f noise, materials with very low or near-zero temperature coefficient of resonant frequency (***τ_F***) are desired. Tuning of τ_F is typically achieved by introducing small levels of impurities that allow the temperature dependence of the dielectric constant to offset the corresponding contribution from thermal expansion. In this project, we investigated the physical and microwave (***ε, tan*** $\boldsymbol{\delta}$ **and** ***τ_F***) properties of microwave dielectrics in order to elucidate the physical mechanisms responsible for limiting their performance in practical microwave technology. The ultimate goal of this effort is to design new materials and processing methods that can enable the manufacture of high-performance microwave dielectric devices with improved quality factors (Q), thermal stability, and manufacturability.

As mentioned in the executive summary, one of our central goals is to understand the fundamental mechanism responsible for the markedly better microwave performance of some dielectric materials over others. Progress towards this objective will enable us to focus on improving the performance of currently-used dielectrics with the greatest potential, as well as to use advanced theory and experiments to systematically design new materials with even better performance. A second central goal is to understand the influence that defects have on the microwave loss mechanism, as many studies have found a correlation between the presence of high defect concentrations and an enhanced loss tangent. The nature of performance enhancing and degrading defects will be uncovered. This information will be used to design material and device processing methods to optimize the material's performance. We have made significant progress towards these goals in our investigation of $Ba(Cd_{1/3}Ta_{2/3})O_3$ (BCT) and $Ba(Zn_{1/3}Ta_{2/3})O_3$ (BZT) under Army Research Office support, as outlined in the following section.

3. Overview of progress under ARO funding
A. Intrinsic materials properties

$Ba(Zn_{1/3}Ta_{2/3})O_3$ is a compound that is widely used in microwave applications because of its large dielectric constant (e ~ 30) and ultralow loss tangent (tan δ < $2x10^{-5}$ at 2 GHz). When $Ba(Zn_{1/3}Ta_{2/3})O_3$ ceramic material is doped with Ni, the temperature coefficient of resonant frequency τ_F can be tuned to near zero. Zr is also commonly used in conjunction with Ni doping because it is found to significantly decrease annealing times required to attain high quality factors (Q), as well as to facilitate high quality factors over a range of stoichiometries. The high manufacturing cost of $Ba(Zn_{1/3}Ta_{2/3})O_3$ is relatively high compared to other dielectrics because of the expensive Ta component. This has limited the use of this compound except in the most demanding applications, such as cell phone base station and satellite communication filters.

$Ba(Zn_{1/3}Ta_{2/3})O_3$ exhibits an unusual combination of a large dielectric constant and a small loss tangent at microwave frequencies. Our recent work using ab-initio electronic structure calculations were able to successfully elucidate the physical reason for the desirable microwave properties of $Ba(Cd_{1/3}Ta_{2/3})O_3$ (BCT), $Ba(Zn_{1/3}Ta_{2/3})O_3$ (BZT) and their alloys. The presence of significant charge transfer between the cation d-orbitals provides a degree of covalent directional

bonding between atoms that resist angular distortions, a property absent in conventional ionic compounds. The angular rigidity strengthens "soft lattice modes" correlated with microwave loss. The bandstructure of BCT and BZT as calculated using the LMTO band structure methodology is illustrated in Figure 1. Charge is transferred from Ta 5d-levels in the conduction band (empty states at and near the CBM) to Cd- 4d and Zn –3d levels (full states at and near the VBM) for BCT and BZT, respectively. This unusual bonding is in contrast to conventional oxides, where the bond is primarily non-directional ionic bonding as a result of the Coulombic forces between highly charged ions in conventional oxide dielectrics. The d-electron bonding in BZT and BCT is responsible for producing a more rigid lattice with higher melting points and enhanced phonon energies than comparable ionic materials. We suggest that this may also be responsible for this class of material's inherently low microwave loss tangent.

In contrast to BZT and BCT, typical high-ε oxides are comprised of ions with large atomic number. The large dielectric constant arises from the highly-polarizable large ions present in such materials. The large separation between atoms (and thus large lattice constants) results in relatively weak non-directional ionic bonds, and thus soft and anharmoic phonons and enhanced microwave loss.

We chose to experimentally investigate BCT and compare it to other tantalite perovskites since initial theoretical calculations predict that the relative contribution of *d*-electron bonding will be stronger in Cd-containing compounds than in the other compounds, including BZT. An important difference that was predicted for BCT is a distortion that results in a bond angle of 172° for the Ta-O-Cd bond. See Figure 1. Our recent X-ray diffraction measurements using advanced Reitvild method to analyze the data determined an angle of 173° (Figure 2 and Table 1 and 2), very near to the LDA theoretical prediction. This was an ***extremely important finding*** as it confirmed the applicability of local density functional calculations for these highly correlated systems.

The oxygen atom bonded between the Ta and Ca ions would be expected to oscillate between the lowest energy positions at room temperature since the energy barrier separating the minima (6 meV) is small compared to thermal energies (26 meV). The associated phonon mode in this direction would therefore be anticipated to have a strong anharmonic component. Experimentally we have confirmed that BCT does have a significantly higher loss tangent than BZT.

In the XRD patterns shown in Figure 2, multiple peaks were found at the high angle diffraction angles. It is well known that B-site ordering occurs in $Ba(B'_{1/3}B''_{2/3})O_3$ perovskites, particularly in samples that have been annealed for a long time. Ordering in the B'-B" lattice produces a distortion from the cubic lattice primarily along the <111> direction which results in the formation of a hexagonal crystal structure. Fitting of the XRD data using Rietveld analysis method indicates that the multiple peaks at high angle are from the mixture of ordered (hexagonal) and disordered (cubic) structures. The weight percentage of the two phases is calculated automatically in the Rietveld analysis. Figure 2 shows the measured (dots) and calculated (line) XRD patterns for the BCT sample doped with 0.1 wt% Ni. The calculated lattice parameters and weight percentages of hexagonal and cubic structures are summarized in Table I which shows that the Ni-doped BCT samples exhibit a small increase in the extent of ordering with increasing Ni concentration. The Bragg reliability factor, R_B, shows the quality of the agreement between observed and calculated profiles. The trend that the lattice parameters decreases with increasing Ni concentrations is expected and fits Vegard's law since the ionic radius of Ni^{2+} is smaller that that of Cd^{2+}
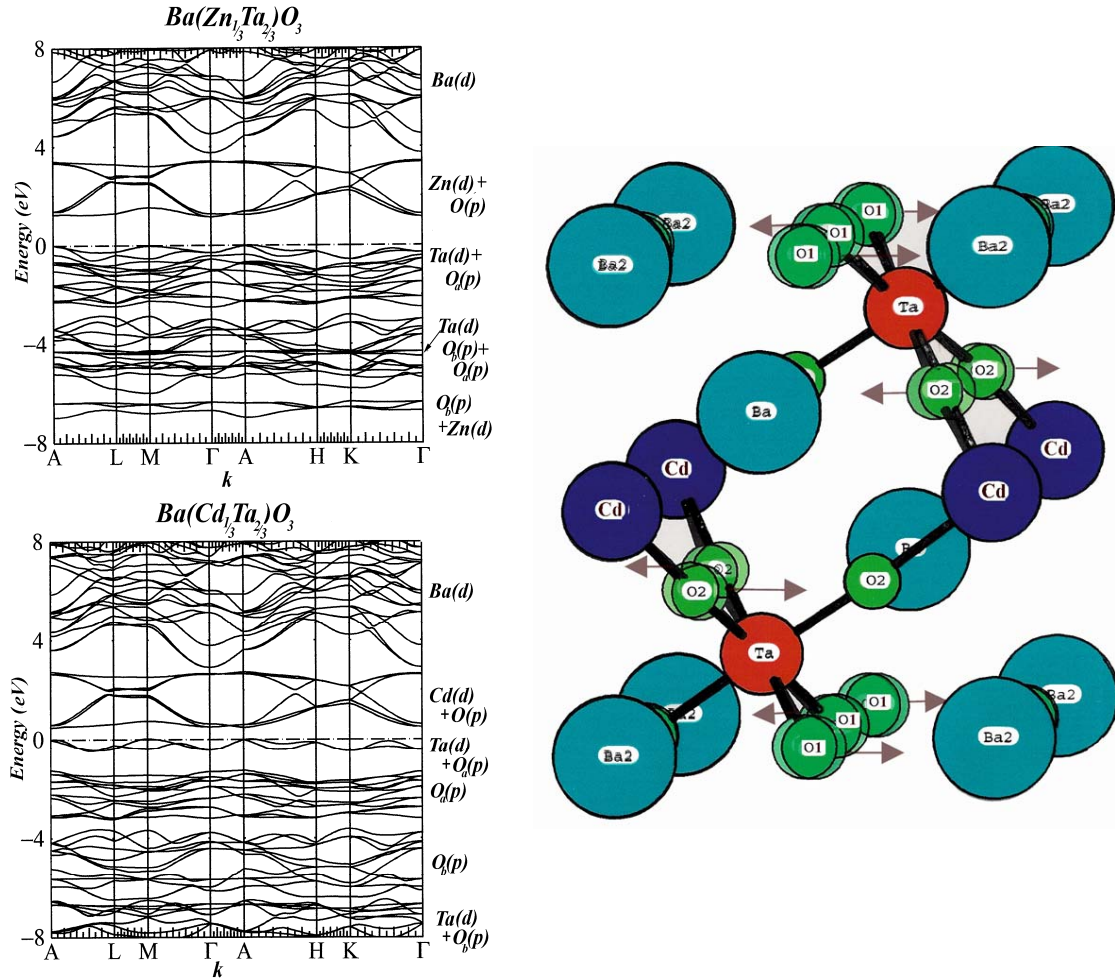
Figure 1. Electronic band structure calculated using the LMTO method for $Ba(Zn_{1/3}Ta_{2/3})O_3$ and $Ba(Cd_{1/3}Ta_{2/3})O_3$. Also shown is the predicted oxygen distortion in the latter compound.

The LDA predicts a bandgap to be 3.26 eV in bulk BZT. Using LDA errors in other oxides as a guide, this estimate is probably 1 to 1.5 eV too low. A screened exchange generalization of the LDA was used to estimate the gap correction (SX is a rather crude way to incorporate the physics of a nonlocal potential found in the GW approximation). The SX result was 4.04 eV. Based on experience with known oxides, this result is also probably also a little low; thus we can expect the BZT bandgap to be ~4.3 eV or so. (As part of our proposed work, we will experimentally pin down this quantity, and attempt to apply GW theory to BZT.) Also we have developed a kind of self-consistent GW approximation, which can address the excitation energies in a much more rigorous framework han the LDA. We have not applied this theory to BZT to date, because it is too expensive to deal with such a large system, but have plans to do so.
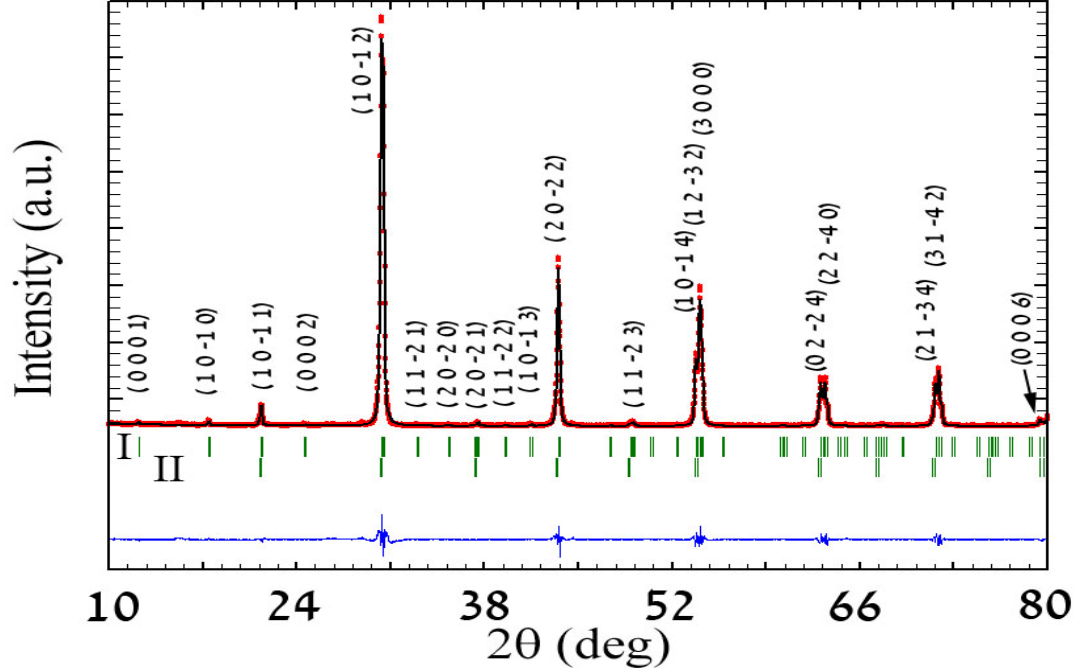
Fig. 2. Rietveld analysis of X-ray diffraction spectra of 0.1 wt% Ni-doped Ba(Cd$_{1/3}$Ta$_{2/3}$)O$_3$ samples. The simulated Bragg peak positions and intensities of ordered (hexagonal, "I") and disordered (cubic, "II") structures are derived using Rietveld analysis and appear as lines. The difference between measured data (dots) and calculated (line) is shown below. The crystallographic planes of the hexagonal structure are given.

Ni (%)	Cubic			Hexagonal					
	a (Å)	R_B (%)	wt%	a (Å)	c (Å)	R_B (%)	wt%	R_{wp} (%)	R_{exp} (%)
0	--	--	--	5.87112(37)	7.24160(61)	15.7	70	27.5	7.63
0.1	4.17492(16)	4.9	6.09(18)	5.86214(9)	7.23296(14)	2.5	93.91(55)	11.1	7.04
0.5	4.17099(22)	8.4	5.31(23)	5.85769(12)	7.22498(18)	3.4	94.69(71)	13.0	8.44
1	4.16969(57)	6.9	4.81(44)	5.84512(18)	7.20308(33)	4.7	95.19(74)	15.7	9.94
2	4.16739(107)	10.7	1.43(5)	5.84110(22)	7.19860(34)	7.3	98.57(271)	23.4	35.59

Table I. Lattice parameters of Ni-doped Ba(Cd$_{1/3}$Ta$_{2/3}$)O$_3$ samples for the cubic and hexagonal structures inferred from Rietveld analysis.

[†] R_B, R_{wp}, R_{exp} in the table are the Bragg R factor, weighted pattern R factor, and expected weighted pattern R factor in Rietveld analysis as defined below.

$$R_B = 100 \frac{\sum |I_{obs} - I_{calc}|}{\sum |I_{obs}|} \quad R_{wp} = 100 \sqrt{\frac{\sum w [y_{obs} - y_{calc}]^2}{\sum w y_{obs}^2}} \quad R_{exp} = 100 \sqrt{\frac{N - P}{\sum w y_{obs}^2}}$$

where y_{obs} and y_{calc} are observed and calculated intensities, I_{obs} and I_{calc} observed and calculated integrated intensities, N number of statistically independent observations, P the number of parameters refined and w the weights associated with y_{obs}.

Table II. Atomic Wyckoff positions of $Ba(Cd_{1/3}Ta_{2/3})O_3$ in space group *P-3m*1 inferred from Rietveld analysis.

Atom	Wyckoff	x	y	z
Ba1	2d	1/3	2/3	0.6627(5)
Ba2	1a	0	0	0
Ta	2d	1/3	2/3	0.1707 (4)
Cd	1a	0	0	½
O1	3e	1/2	0	0
O2	6i	0.1711 (11)	0.8289 (11)	0.3103 (16)

B. The influence of defects in microwave loss

Recent work indicates that defects play a central role in determining the damping constants of the anharmonic modes. It remains unclear whether the observed level of microwave loss in practical dielectrics arises primarily from the presence of point defects or extended defects, although both possibilities have been discussed extensively in the literature. The answer to this question has been elusive because of the presence of a significant concentration of both classes of defects in current state-of-the-art ceramic material.

A significant concentration of point defects, often termed color centers, are present in both BCT and BZT as there is a significant variation in appearance with the samples with large loss tangents being darker in color. Absorption spectra were studied to better quantify this observation. As shown in Fig. 3 and 4, the absorption spectra of Ni doped BCT feature both discrete peaks and varying levels of a continuous absorption background. The discrete peaks in the spectra are similar to those found in Ni-doped BZT, as well as other Ni-containing oxides and are associated with forbidden internal transitions between the Ni d-states. These discrete absorption peaks are absent in undoped BCT samples, as expected. The intensity of the continuous absorption background (a) is responsible for the observed change in color and hue, (b) is caused by point defects and (c) can be directly correlated to the decrease in the loss tangent. This will be discussed later in this section.

Direct evidence that the Ni is incorporated on the Cd sites comes from detailed ligand field analysis. When Ni is incorporated on Cd sites in the BCT lattice, it will be surrounded by oxygen nearest neighbors in an octahedral geometry. According to crystal field theory, the Ni *d*-orbitals are split in a well-defined way by the interaction with oxygen ligand ions located in an octahedreal configuration. This theory can be used to assign the different absorption peaks associated with the in Fig. 3(a) to internal forbidden transition peaks between Ni^{2+} *d* orbitals transitions from the $^2\Gamma_3(F)$ Ni^{2+} ground state to the $^4\Gamma_3(F)$, $^3\Gamma_1(F)$, $^5\Gamma_1(F)$, and $^4\Gamma_3(P)$ excited states. The strength of this interaction, denoted by 10*Dq*, can be inferred from the absorption spectra. As shown in Fig. 3(b), the measured 10*Dq* is 6990 cm^{-1} for 0.1% Ni-doped BCT and 7400 cm^{-1} for 2% Ni-doped BCT. Our earlier publication reported that BZT have 10Dq values of ~7300 cm^{-1} for 0.25% Ni to about 7700 cm^{-1} for 1% Ni. The spectra features occur at relatively higher energies in Ni-doped BZT than in BCT; consistent with the expectation as BCT has a larger lattice parameter than BZT and thus has longer Ni-O bond length in that lattice.

The small amount of absorption from 1.9 eV to 2.3 eV compared to other parts of the visible spectra results in the observed yellow color for the doped BCT samples. High defect concentrations show a marked increase in intensity in all energies above ~1.9 eV, causing the sample to appear a darker yellow/brown color. This observed absorption background in both BZT and BCT is similar to that previously reported in defective single crystal NiO and can be attributed to non-stoichiometry related point defects. We found a clear correlation between the loss tangent

of Ni-doped BZT and BCT samples with the intensity of the continuous absorption background in the optical spectra. This results from the presence of optically active point defects and is indicates that point defects play an important role in the microwave loss in BZT and BCT ceramics.
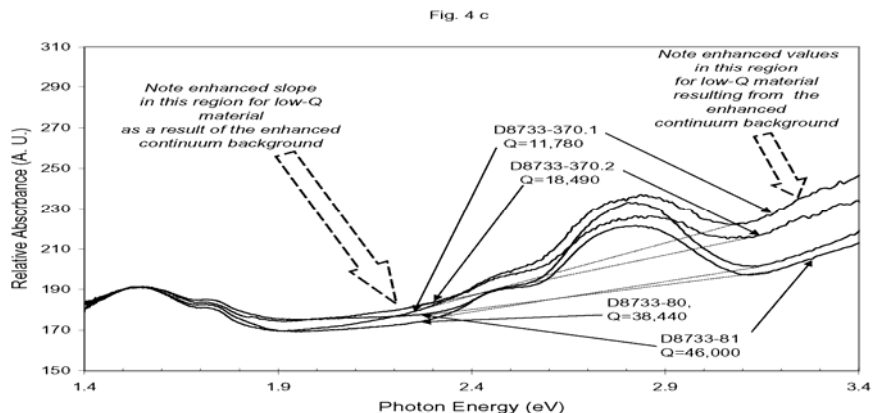

Fig. 3 The results of optical measurements in the visible range for $Ba(Zn_{1/3}Ta_{2/3})O_3$ samples with a wide range of Ni and Zr doping. Note the enhanced background signal for material with diminished quality factors (Qs).
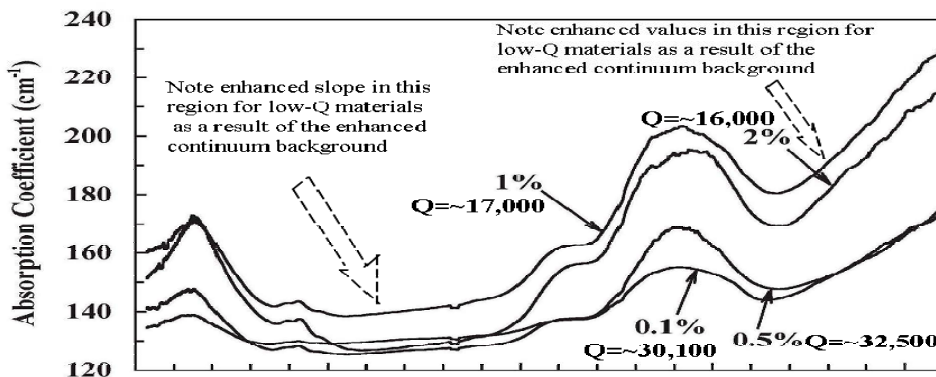
Fig. 4 Visible absorption spectra of $Ba(Cd_{1/3}Ta_{2/3})O_3$ samples doped with varying concentrations of Ni. Note the enhanced background signal for material with diminished quality factors (Qs). The *Q* value of Ni-doped BCT increases with Ni doping up to 0.5 wt% but decreased abruptly when the Ni doping concentration exceeds 1 wt%.

There are several means that can be used to introduce point defects into ceramics samples, including impurity doping, annealing in reducing or oxidizing atmospheres, and high energy particle irradiation. We chose to use radiation damage since it can controllably introduce point defects into the sample without altering other structural parameters, such as crystal structure, porosity, nature and concentration of grain boundaries, dislocations, and/or secondary phases that might significantly affect the dielectric properties of the material. High energy beams were

9

chosen to induce point defects into our ceramics samples because they have a long penetration depth, insuring that they produce a relatively uniform defect distribution. The resulting change in the paramagnetic defect concentration, as monitored by magnetic susceptibility measurements, and the microwave dielectric properties, as measured with microwave dielectric resonator measurements, provides direct evidence of the role that point defects have on the microwave dielectric constant (ε), loss tangent (tan δ) and temperature coefficient of resonant frequency (τ_f). High energy particle irradiation was used to systematically increase the paramagnetic defect concentration by ~34%, with a resulting change of ~5% in the dielectric constant, ~19% in the quality factor and an increase in (τ_F) from zero to ~8ppm/^{o}C.

No significant changes in X-ray diffraction spectra are found after any of the irradiation steps, indicating that there are not any changes in the microstructure of the films upon irradiation. This is consistent with the expectation that this irradiation dose produces predominantly point defects.

Magnetic susceptibility measurements shown in Figure 5 allow us to quantitatively show that a continuous increase in the concentration of paramagnetic point defect in the Ni and Zr-doped Ba(Zn$_{1/3}$Ta$_{2/3}$)O$_3$ samples results with increasing dose of irraditation. The high initial value arises because Ni in Ba(Zn$_{1/3}$Ta$_{2/3}$)O$_3$ lattice is paramagnetic as a result of it's unfilled 3d shell. It has a magnetic moment, μ_e, of 3.223$\pm$0.046. The increase in paramagnetic moment with irradiation can be attributed to the formation of paramagnetic native defects. All samples are found to follow the Curie-Weiss law: $\chi = \dfrac{C}{T - \Theta}$ where C is the Curie constant and Θ is the Curie temperature. The paramagnetic defect concentration is then inferred and designated in Figure 5.

Figure 6 indicates the effect of irradiation damage on the dielectric properties of the Ni and Zr-doped Ba(Zn$_{1/3}$Ta$_{2/3}$)O$_3$ samples. Figure 6(a) and (b) show the dielectric constant (ε_r) and quality factor (Q) decrease continuously with the extended damage respectively. Since a change in the microstructure is not detected in the XRD analysis, we conclude that these changes in the dielectric properties can be attributed to the appearance of additional native defects resulting from the irradiation. The drop in the quality factor with increasing irradiation dose is consistent with our earlier conclusion that the loss tangent of the material depends strongly on the point defect concentration.

Figure 6(c) shows that the point defects also affect the temperature coefficient of resonant frequency. The appearance of point defects increases the value of the temperature coefficient of resonant frequency from near zero to ~8 ppm/^{o}C. This suggests that the presence of point defects may also play a role in establishing the temperature coefficient of resonant frequency. We did not find evidence for secondary phases in the XRD data, another important factor that has been shown to influence the temperature coefficient of resonant frequency of other microwave dielectrics, e.g. Ba(Cd$_{1/3}$Ta$_{2/3}$)O$_3$, Ba$_2$Ti$_9$O$_{20}$ and MgTiO$_3$-CaTiO$_3$. Earlier experimental results have also found that, the temperature coefficient of resonant frequency can be directly correlated to the nature and extent of B-site ordering in ABO$_3$ perovskites, as reported in a study of Ba$_x$Sr$_{1-x}$(Zn$_{1/3}$Nb$_{2/3}$)O$_3$. However, X-ray diffraction results from our study do not find large changes in the degree of ordering in the material.
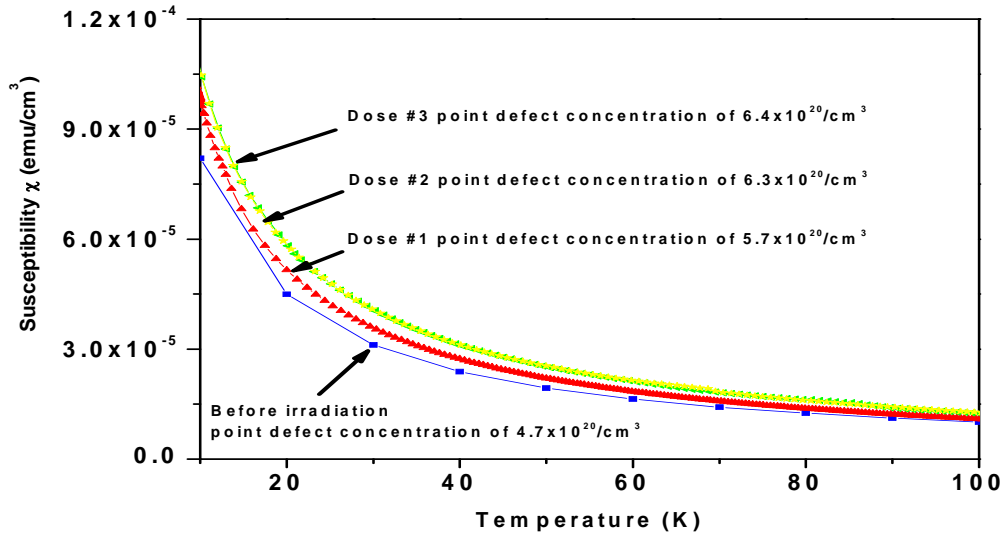
Figure 5 The magnitude of the observed paramagnetic moment of the Ni and Zr-doped Ba(Zn$_{1/3}$Ta$_{2/3}$)O$_3$ samples as a function of irradiation dose. The concentration of paramagnetic point defects inferred from fitting the Curie-Weiss law is also included.

In summary, irradiation damage has significant effect on the dielectric properties of Ni and Zr-doped Ba(Zn$_{1/3}$Ta$_{2/3}$)O$_3$ samples with composition Ba(Ni$_{0.125}$Zr$_{0.1275}$Zn$_{0.845}$Ta$_{1.940}$)O$_3$. Magnetic results show that the increase paramagnetic moment is due to the appearance of paramagnetic native point defects resulting from the irradiation. The appearance of point defects decreases the dielectric constant and quality factor. In contrast, the temperature coefficient of resonant frequency is increased from near zero to 8 ppm/^{o}C. Additional work is underway to elucidate the atomic nature of the defects that have been created during the irradiation process.

C. Defects, Theory
Our prior work was aimed towards the energetics of defects in BZT, based on calculations with the local-density approximation. LDA calculations were carried out using a generalization [1] of the standard [2] method of linear muffin-tin orbitals (LMTO).
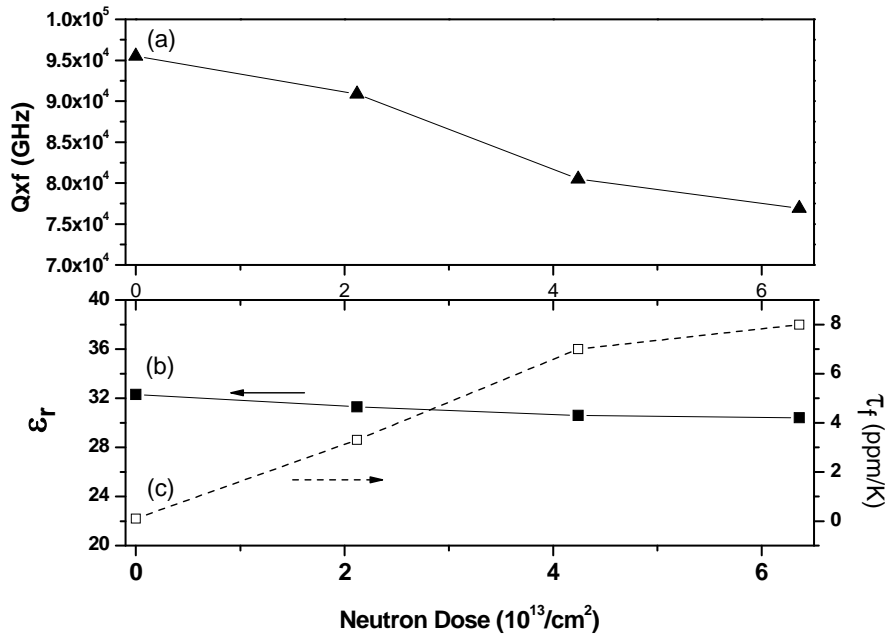
Figure 6 Effect of irradiation damage on the dielectric properties of Ni and Zr-doped Ba(Zn$_{1/3}$Ta$_{2/3}$)O$_3$: (a) Dielectric loss; (b) Dielectric constant; (c) Temperature coefficient of resonant frequency (τ_f).

We focused on three types of native point defects: vacancies, Frenkel defects (vacancies + interstitials), and Schottky defects (donor and acceptor pair, which mutually compensate each other). In these calculations we used a 60 atom (4×15 atom) supercell. Within the cell, all atomic positions were relaxed (relaxation energies are typically very large). Two kinds of properties were investigated: energetics (ground state) and energy levels (excited state property), particularly defect levels. The LDA is reasonably good for the former, but it has a well-known tendency to underestimate, e.g. bandgaps. Thus there is some uncertainty about the position of defect levels.
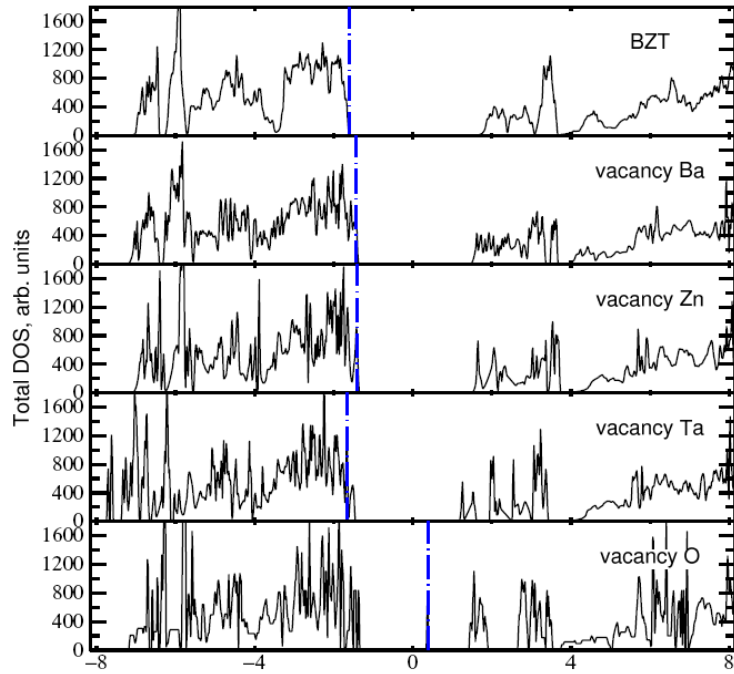
Figure 7. Densities-of-states of the four kinds of vacancies in BZT, compared to DOS of bulk BZT (top). The DOS were aligned to the core levels; the Fermi level is shown as a dashed blue line.
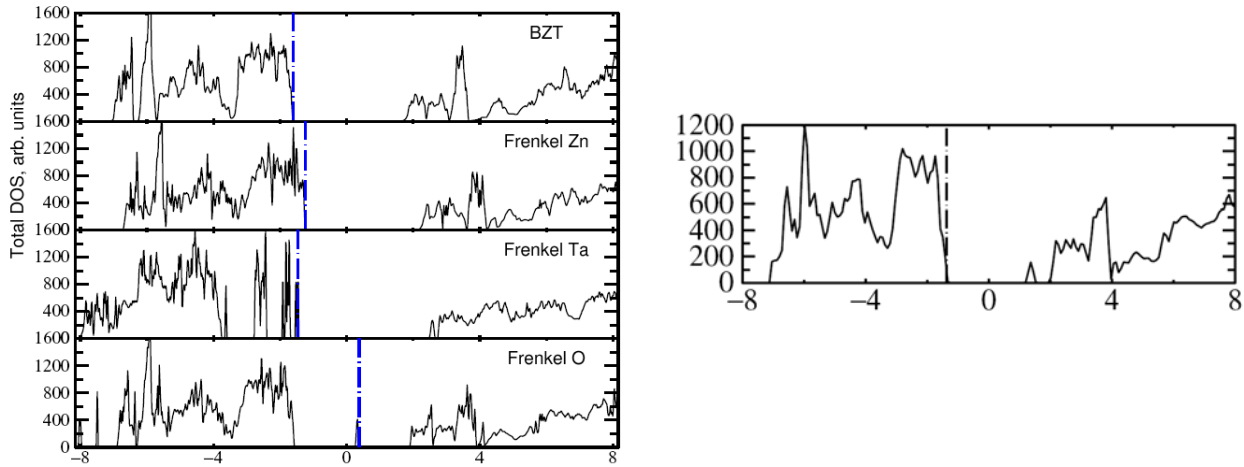
Figure 8. Left: Densities-of-states of the Frenkel defects in BZT, compared to DOS of bulk BZT (top). The DOS were aligned to the core levels; the Fermi level is shown as a dashed blue line. Right DOS of the V_{Ba} +V_O Schottky defect.

Figure 7 shows densities of states (DOS) of the simple vacancies. V_{Ba}, V_{Zn} and V_{Ta} are shallow acceptors, as can be seen by the fact that the valence band top "spills out" above the VBM of bulk BZT (marking the position of the acceptor level). Ba and Ta are double-acceptors (filled level); Ta leaves behind five holes (E_F falls below valence band top) V_O is a deep donor, located

13

1.6 eV below the conduction band in the LDA. All simple vacancies have very large formation energies: e.g. within the LDA we obtain ~8 eV (V_{Zn}) and ~19 eV (V_{Ta}).

Figure 8 shows DOS of the Frenkel defects. Ba is not shown because it was found to be unstable: starting from its interstitial site, it finds a continuous path back to the vacancy position it left behind without encountering any local minima on the path. Surprisingly, we found that the Zn Frenkel is less stable than the separated interstitial + vacancy. In any case, the defect was found to be extremely costly (~26.6 eV); thus we can rule it out as a likely defect. The Ta Frenkel has a low formation energy (~1.5 eV); thus it is a likely candidate for defect formation. The O Frenkel (~7.4 eV) is (~3.7 eV less costly than the isolated interstitial + vacancy. Interestingly the donor level of the vacancy and the Frenkel lie at approximately the same position (E_c −1.6 eV)

We also considered some Schottky defects, e.g. V_{Ba} +V_O. It might be expected that they compensate (combining donor and acceptor). Fig. 8 shows that this is the case. A shallow level forms at E_c−0.6eV according to the LDA. (But since the LDA cannot reliably predict gaps, we cannot determine whether this prediction is reliable without a method that goes beyond the LDA). Its formation energy was found to be ~5.5 eV.

Finally, we considered Ta antisites on Zn. The energy of formation is very low, which that it is difficult to stabilize stoichiometric BZT (there will tend to be a Zn deficiency). This analysis will be carried out in detail in future studies.

Impurity Defects: We considered the charge-neutral substitution : 2 Ta + 1 Zn → 3 Zr . This can probably be synthesized since it is charge-neutral. The gap was reduced by ~0.7 eV. Thus, addition of Zr into the powder should make it possible to systematically control the bandgap. Ni is added to BZT in small amounts to stabilize the microwave frequency. We find that it generates two kinds of deep levels, and it also narrows the fundamental gap.
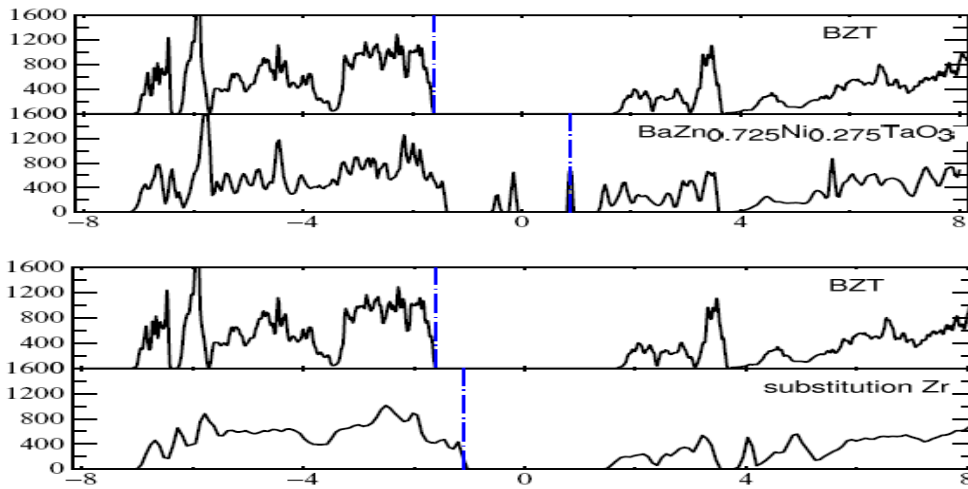

Figure 9. DOS of Zr: and Ni: doped BZT as described in the text.

D. Fabrication of single-crystal thin films for characterization studies:

To map bandstructure using the well established techniques of photoemission and inverse photoemission, clean single crystal surfaces are required. This is also important for many other studies including optical transmission and reflection studies as polycrystalline samples are challenging to characterize as a result of scattering from grain boundaries and other extended defects. To attain high quality single crystals, Ni and Zr-doped Ba(Zn$_{1/3}$Ta$_{2/3}$)O$_3$ films have been

epitaxially grown on MgO (100) substrate by Pulsed Laser Deposition (PLD). Zn capping layers can be used to protect the surface from contamination during transfer through the atmosphere to the characterization systems, analogous to the As capping methods used for GaAs samples.

To produce high quality BZT films using Pulsed Laser Deposition, elevated substrate temperatures were used to overcome the kinetic barriers of thin film growth (e.g. surface diffusion and reaction) and thus produce high-crystalline-quality epitaxial layers. Under these conditions, substantial Zn loss occurred which could be successfully compensated for by using a Zn-enriched target in combination with enhanced oxygen growth pressures (which act to form less volatile oxidized zinc surface species). To our knowledge, this is the first time single crystal thin films of high-performance microwave material have been synthesized.

We have synthesized and characterized epitaxial and stoichiometric $Ba(Zn_{1/3}Ta_{2/3})O_3$ (100) dielectric thin films grown on MgO (100) substrates by Pulsed Laser Deposition (PLD). Zn-enriched targets and high oxygen pressures are used to compensate for Zn loss during film growth. The $Ba(Zn_{1/3}Ta_{2/3})O_3$ films have an indirect optical band gap of ~3.0 eV and a refractive index of 1.91 in the visible spectral range. A dielectric constant of 25 and dissipation factor of 0.0025 at 100 kHZ has been measured using the interdigital capacitor method. The $Ba(Zn_{1/3}Ta_{2/3})O_3$ films exhibit a small thermally-activated Ohmic leakage current at high fields (<500 KV/cm) and high temperatures (<200 °C) with an activation energy of 0.85 eV.

In this study, we report the successful growth of epitaxial and stoichiometric $Ba(Zn_{1/3}Ta_{2/3})O_3$ (100) films on MgO (100) substrates and the results of structural, chemical, optical and electrical characterization.

An Ultra-High Vacuum (UHV) Pulsed Laser Deposition (PLD) system was used to deposit $Ba(Zn_{1/3}Ta_{2/3})O_3$ (100) thin films on single crystal MgO (100) substrates. The PLD system is equipped with a KrF excimer laser (Lambda Physik, λ=248 nm) operated at an energy of 450 mJ/pulse and a repetition rate of 2 Hz. The base pressure of the vacuum chamber was ~5×10^{-7} Torr before film growth. The substrate-target distance was ~5 cm. The oxygen pressure during growth was kept at between 50 mTorr and 500 mTorr.

Two different targets were used in the films growth. The first was a stoichiometric commercial target doped with Zr and Ni with composition $Ba_3(Zn_{0.845}Ta_{1.94}Ni_{0.125}Zr_{0.09})O_9$ (Trans-Tech Inc., Adamstown, Maryland). The second was a Zn-enriched target comprised of a homogeneous mixture of 1 mole of $Ba_3(Zn_{0.845}Ta_{1.94}Ni_{0.125}Zr_{0.09})O_9$ and 0.75 mole of ZnO. It was produced in our lab using conventional ceramic powder processing techniques with high purity reagents (>99.5%).

The films composition and thickness was determined by Rutherford Backscattering Spectroscopy (RBS) with 3.05 MeV He^+ incident beam. RBS analysis was performed using the RUMP software package (Rutherford Backscattering Spectroscopy Analysis Package, Genplot, Cortland, OH). X-ray diffraction (Rigaku D/MAX-IIB, Japan) and channeling Rutherford Backscattering Spectroscopy (c-RBS) were used to characterize the structural properties of the thin-films. The optical properties were characterized with a double channel spectrometer (Model DS200, Ocean Optics Inc., Dunedin, Florida). The absorption coefficient was inferred from the measured absorbance and sample thickness.

To study the electrical properties, an interdigital configuration was patterned with a Au/Ti bi-layer on the BZT/MgO films. The frequency, temperature and field-dependence of the dielectric constant and dissipation factor were studied using a RLC meter (QuadTech 7400 Precision RLC Meter, Maynard, Maryland). Electrical D.C. bias was applied to the $Ba(Zn_{1/3}Ta_{2/3})O_3$ interdigital structure from positive to negative voltage and back again. The C-V measurements were conducted at room temperature with a 100 KHz A.C. signal frequency. The leakage-current

characteristics were studied using a high resistance/insulation properties measurement instrument (QuadTech 1865 Megohmmeter/IR tester, Maynard, Maryland).

Figure 10(a) summarizes the composition of as-grown $Ba(Zn_{1/3}Ta_{2/3})O_3$ films synthesized from the stoichiometric target with an oxygen working pressure of 200 mTorr. When the substrate temperature is higher than 400 °C, a substantial Zn-loss occurs, which is found to monotonically increase with temperature.

It is well known that the PLD process is able to dispel a stoichiometric composition from the target because of the laser pulse's high energy flux and its small absorption length in the target. However, Zn, which has a significantly larger vapor pressure than the other elements in BZT, may either not stick to or be re-evaporated from the growing surface. A deficiency in the most volatile element is also commonly observed in other films grown by PLD, including K in $KTa_{(1-x)}Nb_xO_3$ [12], Pb in $Pb(Zr_xTi_{1-x})O_3$ [13] and Li in $LiNbO_3$[14]. The composition of less volatile elements (e.g. Ba, Ta, Ni and Zr) in the deposited films is found to be close to that in the target.

Our experiments found that the use of enhanced levels of oxygen working pressure during growth could decrease the Zn loss. Firstly, high oxygen pressure enhances the Zn-O bond formation on the growing surface, and these chemically reacted species are significantly less volatile than Zn metal. Secondly, the kinetic energy of the impinging species at the growth surfaces decreases at higher pressures as a result of scattering, which will reduce the degree of sputtering of elemental Zn and Zn-containing species. The volatilization of Zn during high temperature sintering of $Ba(Zn_{1/3}Ta_{2/3})O_3$ and related compounds indicates that the Zn-O bond is not as strong as Ba-O or Ta-O bonds, thus selective sputtering appears likely. In addition, the use of high oxygen pressures suppresses the atoms surface diffusion as a result of the decrease in the kinetic energy of impinging reactant species at the growth surface, which can result in degradation of epitaxial film quality.

The structures of these films were characterized by X-ray diffraction (XRD), as shown in Figure 10(b). At room temperature, there was no evidence of $Ba(Zn_{1/3}Ta_{2/3})O_3$ diffraction peaks, indicating an amorphous or nanocrystalline structure. At high substrate temperatures (T > 400 °C), we observed the presence of $Ba(Zn_{1/3}Ta_{2/3})O_3$, $Ba_4Ta_2O_9$ and Ta_2O_5 phases. The same products are also found after $Ba(Zn_{1/3}Ta_{2/3})O_3$ decomposition that occurs during the high temperature sintering process.

It is thus clear that *in-situ* growth of single phase $Ba(Zn_{1/3}Ta_{2/3})O_3$ film is very challenging, primarily because of the high Zn volatility. In the following section, we will show that near-stoichiometric single phase $Ba(Zn_{1/3}Ta_{2/3})O_3$ films can be successfully grown on MgO (100) substrates when high oxygen working pressures and Zn-enriched target are used.

The next batch of $Ba(Zn_{1/3}Ta_{2/3})O_3$ films that we will describe were grown from a Zn-enriched target [$Ba(Zn_{1/3}Ta_{2/3})O_3$:ZnO = 4:3] with otherwise similar conditions to that used before. The results of RBS composition analysis and XRD characterization of these films grown are shown in Figure 11. It is clear that the Zn/Ta ratio monotonically decreases with increasing substrate temperature, as was observed during growth from the stoichiometric target. However, for this batch, the Zn/Ta ratio systematically ranged from being below to above the desired ratio of 1:2, as a result of the compensation made in the target. XRD characterization found that single-phase (*l00*) $Ba(Zn_{1/3}Ta_{2/3})O_3$ films can be epitaxially grown on (100) MgO substrate when the substrate temperature is set in the range of 500 to 700 °C. A RBS channeling coefficient, χ, as low as 25% was observed when the substrate temperature is 600 °C. The calculated in-plane lattice parameter of the 250 nm thick pseudocubic $Ba(Zn_{1/3}Ta_{2/3})O_3$ thin film grown at 600 °C is about 4.104 Å. This can be compared to the bulk value of 4.089 Å, indicating that the $Ba(Zn_{1/3}Ta_{2/3})O_3$ films have an in-plane tensile strain.

The peaks associated with Zn-Ta B-site ordering are not observed in the $Ba(Zn_{1/3}Ta_{2/3})O_3$ film X-ray diffraction data. This presumably results because the substrate temperature during growth is not sufficiently high to provide the required thermal energy for surface and bulk diffusion. This is not unexpected since high temperatures (>1400 °C) and long sintering times (>10 hours) are needed to form B-site ordering in bulk $Ba(Zn_{1/3}Ta_{2/3})O_3$ ceramics. This may also be asseverated by the presence of small levels of nonstoichiometries in the as-grown film, particularly with regard to the Ta/Zn ratio.

The band gap is one of the most important intrinsic properties of semiconductors and insulators. To the best of our knowledge, the energy of the $Ba(Zn_{1/3}Ta_{2/3})O_3$ band gap has not been previously reported. Optical characterization is the most convenient technique to determine the band gap of materials. For parabolic bands near the band extrema, the relationship between the optical band gap energy E_g and films absorption coefficient can be determined using Tauc's plot: $\alpha h v \propto (h v - E_g)^n$ where n=$^1/_2$ for direct band gap and n=2 for indirect band gap materials. A linear Tauc region is found for materials with a parabolic density-of-state distribution just above the optical absorption edge. Extrapolation of this line to the photon energy axis yields the optical band gap energy.

Recent Local Density calculation indicated that $Ba(Zn_{1/3}Ta_{2/3})O_3$ is an indirect band gap material with Ta 5-d level in the conduction band minimum and a combination of the O 2-p and Zn 4-d level in the valence band maximum. It can readily be observed that more than one band extrema will contribute to the near-band edge absorption and these bands are not parabolic with energy in this region, so a traditional Tauc's plot can not be used.

In figure 12(a), we show the absorption spectra for our best $Ba(Zn_{1/3}Ta_{2/3})O_3$ thin films, as judged by the epitaxial quality and stoichiometry. It is well known that the presence of small levels of native and impurity defects and strain can make significant contributions to the optical spectrum, particularly within the bandgap of the host material. Since the nature and concentration of such defects have not been characterized in these single-crystal thin films, we will compare the optical results of the single-crystal thin-film samples with those on high-quality powder and ceramic materials, because the latter has been well established that they are stoichiometric and have a relatively small defect density.

To infer an absorption coefficient for measurements on ceramic samples, we will first discuss our results using diffuse reflectance measurements on ceramic $Ba(Zn_{1/3}Ta_{2/3})O_3$. Kubelka-Munk theory[18] is used to analyze the data with the equation $F(R_\infty) = \frac{(1-R_\infty)^2}{2R_\infty} \propto \frac{\alpha}{s}$, where R_∞ is the diffuse reflectance from an infinitely thick sample, α is the absorbance and S is the scattering factor (which is relatively independent of wavelength for sample particle size greater than the light wavelength). Kubelka-Munk theory assumes that (a) the strong optical scattering limit occurs in the measured samples and (b) scattering is isotropic. This approach has proven to give reliable results on ceramic $Ba(Zn_{1/3}Ta_{2/3})O_3$ in reference 4.

Figure 12(b) and 3(c) illustrate the Kubelka-Munk function of pure $Ba(Zn_{1/3}Ta_{2/3})O_3$ and Ni and Zr doped $Ba(Zn_{1/3}Ta_{2/3})O_3$ ceramics, respectively. This can be directly compared to the absorbance spectrum of the thin film. In the doped $Ba(Zn_{1/3}Ta_{2/3})O_3$, a peak at 2.77 eV is observed that corresponds to the d to d forbidden transition from the Ni $^3\Gamma_2(F)$ ground state to the $^4\Gamma_3(P)$ excited state. This transition has been found to produce the largest peak in this spectral region and is observed at an energy consistent with that reported in Reference 4. Based on the absorbance spectrum of figure 12(a), (b) and (c), we tentatively estimate the bandgap of $Ba(Zn_{1/3}Ta_{2/3})O_3$ to be around 3.0 eV.

The transmission intensity through a relatively thick sample (~0.3mm) of sintered polycrystalline Ba(Zn$_{1/3}$Ta$_{2/3}$)O$_3$ ceramics was also measured. Despite the simplicity of the experiment, an accurate determination of the optical parameters by transmission measurements of polycrystalline samples is not straightforward, because transmitted light will undergo multiple scattering events as it travels through the sample. This results in an effective path length that is larger than the sample thickness and prevents an absolute magnitude determination of the absorption coefficient. It also results in a significant reduction in the intensity of the transmitted signal being backscattered out the front surface. Evidence from this effect comes from the disproportionately larger intensities observed in absorbance for the sub-bandgap light. In order to minimize the influence of this artifact, we have subtracted out the linear background, as shown in Figure 12(d) interested. The corrected absorbance spectrum of polycrystalline Ba(Zn$_{1/3}$Ta$_{2/3}$)O$_3$ sample is very similar to that for the single-crystal thin-films and for the Kubelka-Monk function of the powder and ceramic, validating that the procedure of subtracting the background is reasonable. Figure 12(e) is the LDA calculated absorption coefficient of Ba(Zn$_{1/3}$Ta$_{2/3}$)O$_3$, and the photon energy axis was shifted down 0.7 eV to match the absorption peaks of measurement and calculation. This density functional calculation only includes the direct transition. From these results, we conclude that the indirect bandgap is at 2.95 $\pm$ 0.10 eV and a strong direct transition is found at ~3.5 eV. .

Figure 13 illustrates the transmission spectrum of Ba(Zn$_{1/3}$Ta$_{2/3}$)O$_3$ films grown from Zn-enriched target at 600 °C. The transmission coefficient of Ba(Zn$_{1/3}$Ta$_{2/3}$)O$_3$ films in the visible light frequency range is over 60%. The materials complex refractive index $\eta = n - ik$ can be inferred from the optical transmittance. By fitting the extrema in the oscillations that result from interference between reflections the surface and interface with the substrate, two smooth curves of T_{max} and T_{min} can be generated (dashed line in Figure 13). In the case of weak absorption (showed in figure 12) and assuming T_{max} and T_{min} to be a continuous function of wavelength, we can use the following equations to infer a refractive index for Ba(Zn$_{1/3}$Ta$_{2/3}$)O$_3$ films to be ~ 1.91 in the visible light range.

$$n = [N^2 + (N^2 - n_0{}^2 n_1{}^2)^{1/2}]^{1/2} \qquad (2)$$

and

$$N = \frac{n_0{}^2 + n_1{}^2}{2} + 2n_0 n_1 \frac{T_{\max} - T_{\min}}{T_{\max} T_{\min}} \qquad (3)$$

n, n_0 and n_1 are the refractive indexes of the Ba(Zn$_{1/3}$Ta$_{2/3}$)O$_3$ films, air and MgO substrate, respectively.

C. Electric characterization

The dielectric properties of Ba(Zn$_{1/3}$Ta$_{2/3}$)O$_3$ thin films have been characterized using an interdigital structure. A standard lift-off technique was used to lithography-pattern Ti/Au interdigital electrodes on the Ba(Zn$_{1/3}$Ta$_{2/3}$)O$_3$ films. The interdigited structure consisted of 40 fingers that were 2 mm long and 20 μm wide and were separated by their symmetric partner by 20 μm. A Quadtech 7400 LRC Impedance meter was used to measure the effect of frequency, bias and temperature on the dielectric properties in these Ba(Zn$_{1/3}$Ta$_{2/3}$)O$_3$ thin-film structures. The dielectric constant of Ba(Zn$_{1/3}$Ta$_{2/3}$)O$_3$ films could be derived from the Farnell conformal mapping method. The dielectric constant of the substrate ε_s and the films ε_f can be formulated:

$$\varepsilon_f = \varepsilon_s + \frac{C/K - (\varepsilon_s + 1)}{1 - e^{-4.6/(h/L)}} \qquad (4)$$

$$\varepsilon_s = \frac{C_s}{K} - 1 \qquad\qquad (5) \qquad K = 6.5(D/L)^2 + 1.08D/L + 2.37$$

$$(6)$$

where C_s (pF/m) and C (pF/m) are the measured capacitances per meter for an isolated substrate and the films positioned on a substrate, respectively; h is the film thickness L is the interdigital finger pitch width; K is an empirical value and D is the finger width.

Figure 14 shows the room-temperature dielectric constant and dissipation factor of a $Ba(Zn_{1/3}Ta_{2/3})O_3$ films grown at 600 °C from a Zn enriched target for frequencies ranging from 1 – 100 kHz. The dielectric constant is inferred to be 25, which is comparable with that of the bulk ceramics of ~28-30. The loss tangent is determined to be 0.002-0.004, corresponding to a quality factor (Q) of over 250. This is presumably a lower bound as it the measured value may be dominated by losses in the metal. This Q value is nevertheless much higher than $Ba(Mg_{1/3}Ta_{2/3})O_3$ films made by metalorganic solution deposition or PLD grown $Ba(Mg_{1/3}Ta_{2/3})O_3$ amorphous films followed by annealing-induced crystallization.

The thermal stability of the capacitance of $Ba(Zn_{1/3}Ta_{2/3})O_3$ in these interdigital strucures has been investigated in the temperature range from 25 to 200 °C at a. signal frequency of 100 kHz. Figure 15 shows the capacitance monotonically increases with increasing temperature. For bulk $Ba(Zn_{1/3}Ta_{2/3})O_3$ ceramics, Ni doping was used to offset the effect of thermal expansion with that of the temperature dependence of the dielectric constant in the microwave frequency region, thus achieving near zero τ_f in microwave filter and resonator structures. For the $Ba(Zn_{1/3}Ta_{2/3})O_3$ interdigital capacitors, the problem is more complicated because the thermal expansion of the $Ba(Zn_{1/3}Ta_{2/3})O_3$ films is restricted by the MgO substrate and top Ti/Au layer (α_{Ti} = 8.6 ppm/K; α_{Au} =14.2 ppm/K; α_{MgO}=12.8 ppm/K [MTI Corp.] and α_{BZT} =10 ppm/K [Trans-tech Corp.). The measured temperature coefficient of $Ba(Zn_{1/3}Ta_{2/3})O_3$ interdigital capacitance is ~71 ppm/K. The dissipation factor of $Ba(Zn_{1/3}Ta_{2/3})O_3$ films increases slightly with temperature, as shown in Figure 15.

Figure 16 shows the C-V characteristics of $Ba(Zn_{1/3}Ta_{2/3})O_3$ films measured using the interdigital configuration. The capacitance and dissipation factor do not exhibit significant changes with bias, at least up to 50 kV/cm.

Figure 17 illustrates the I-V characterization of $Ba(Zn_{1/3}Ta_{2/3})O_3$ films in the interdigital configuration as a function of temperature. The linear I-V relationship indicates that the Ohmic conduction mechanism persists up to fields of 500 KV/cm and temperatures of 200 °C. Figure 18 plots the log(I)-1/T relationship of the Ohmic leakage currents at a 100 kV/cm field. The leakage currents obey Arrhenius dependence according to $I = I_0 \exp(-E_a/KT)$. Activation energy of 0.85 eV is inferred from the analysis.

Epitaxial and stoichiometric $Ba(Zn_{1/3}Ta_{2/3})O_3$ (001) dielectric films were grown on MgO (100) substrates using pulsed laser deposition using a Zn-enriched target and elevated oxygen pressures. The structural, chemical, optical and electrical properties of $Ba(Zn_{1/3}Ta_{2/3})O_3$ films were investigated. The $Ba(Zn_{1/3}Ta_{2/3})O_3$ films has an optical direct band gap of ~3.0 eV, and a refractive index of ~1.91 in the visible range. The dielectric constant and dissipation factor of $Ba(Zn_{1/3}Ta_{2/3})O_3$ thin films at room temperature are measured to be 25.0 and 0.0025, respectively. The dielectric characteristics of $Ba(Zn_{1/3}Ta_{2/3})O_3$ films exhibited excellent bias and temperature stability. The leakage current of $Ba(Zn_{1/3}Ta_{2/3})O_3$ follows an Arrhenius relationship with an activation energy of 0.4 eV at temperatures up to 200 °C and electric fields up to 500 KV/cm field. The structural compatibility and the excellent optical and electrical properties makes $Ba(Zn_{1/3}Ta_{2/3})O_3$ films a promising candidate for use in a number of potentially useful microelectronic and microwave communication applications.

Figure 10(a). Elemental composition in as-grown films fabricated using a stoichiometric Ba(Zn$_{1/3}$Ta$_{2/3}$)O$_3$ target; (b)X-ray diffraction data of the same films grown over a range of substrate temperatures.

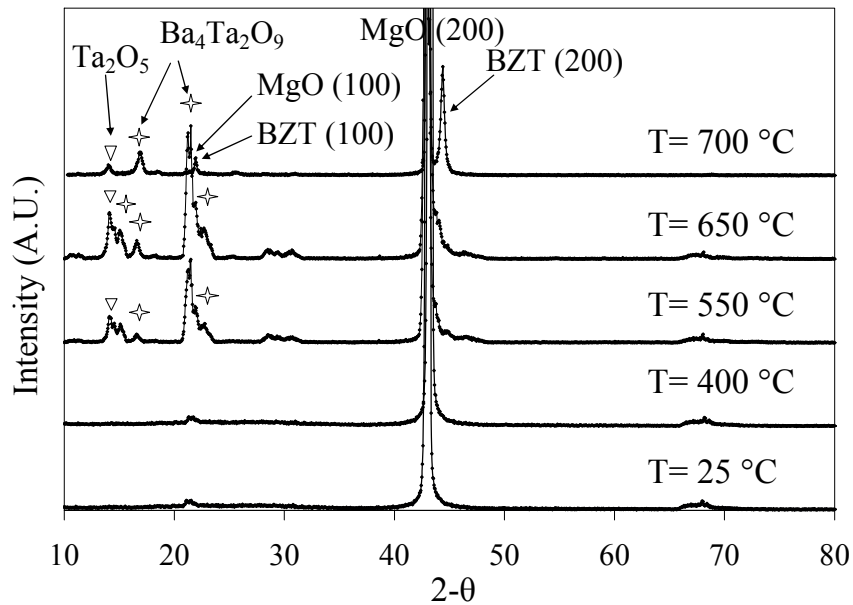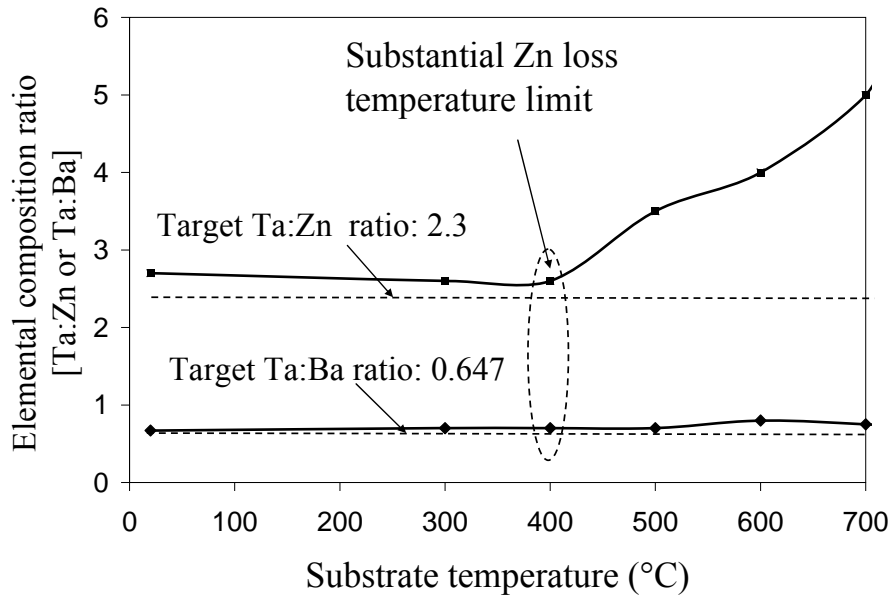**Figure 11.** X-ray diffraction data of the $Ba(Zn_{1/3}Ta_{2/3})O_3$ films grown at different substrate temperatures from a Zn-enriched target, and their corresponding compositions as inferred by RBS analysis. The Ni and Zr atomic concentrations in the as-grown films are ~3 at.%, very near to that in the target
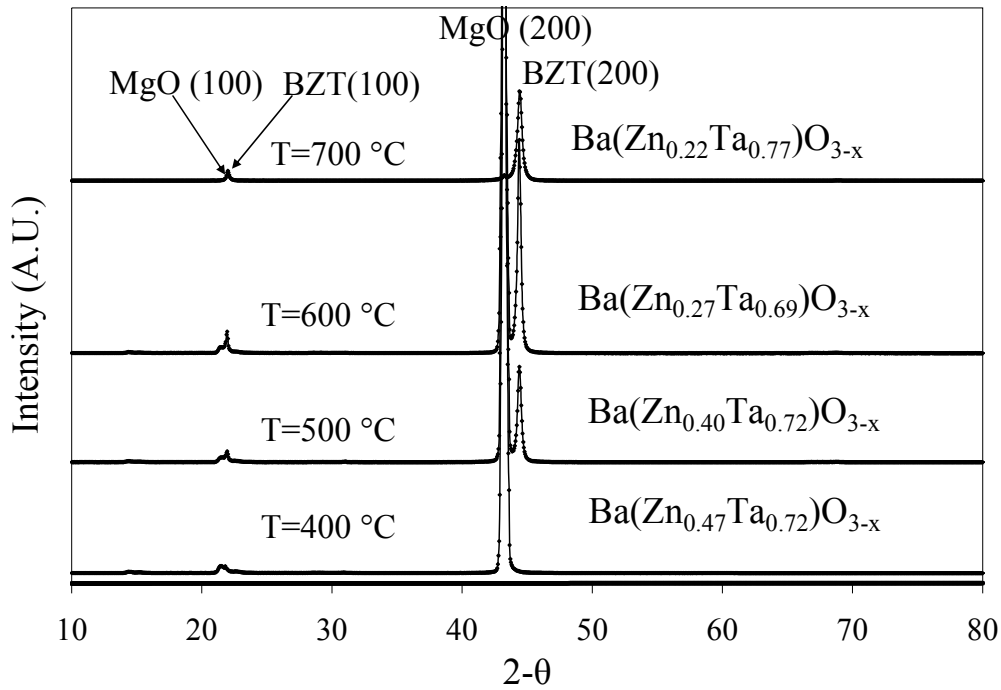
Figure 12. (a-e) Optical characterization of Ba(Zn$_{1/3}$Ta$_{2/3}$)O$_3$ thin film, ceramics and bulk polycrystalline material.
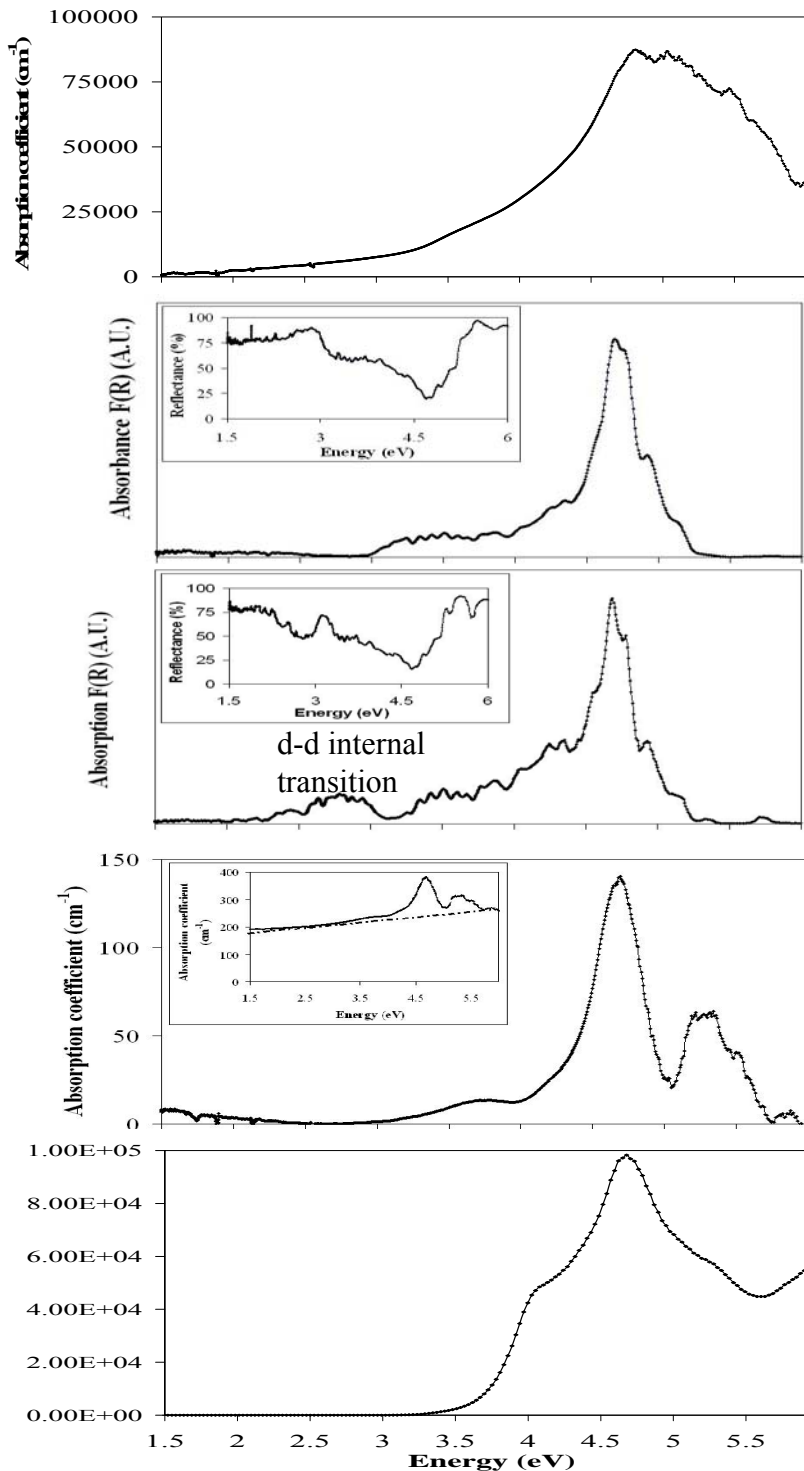
(a) Absorption spectrum of Ni and Zr (both ~3at.%) doped BZT films grown on MgO absorption spectrum at 600 °C using the Zn-enriched target

(b) Kubelka-Munk function for pure BZT ceramics, the inserted is original diffuse reflectance

(c) Kubelka-Munk function for Ni and Zr doped BZT ceramics, the absorbance bump at 2.77 eV is the Ni d-d Ni $^3\Gamma_2$(F) to the $^4\Gamma_3$(P) transmition . Inserted is original diffuse reflectance

(d) Corrected absorbance spectrum of pure BZT polycrystalline ceramics (~0.3mm thick). The original spectrum is showed as inserted and the background was subtracted as the dashed line.

(e) Calculated absorption spectrum shifted 0.71 eV to low energy direction, to make the highest peak lines up with the experimental peaks

Figure 13. Transmission spectrum of Ba(Zn$_{1/3}$Ta$_{2/3}$)O$_3$ films grown at a 600 °C substrate temperature using a Zn-enriched target
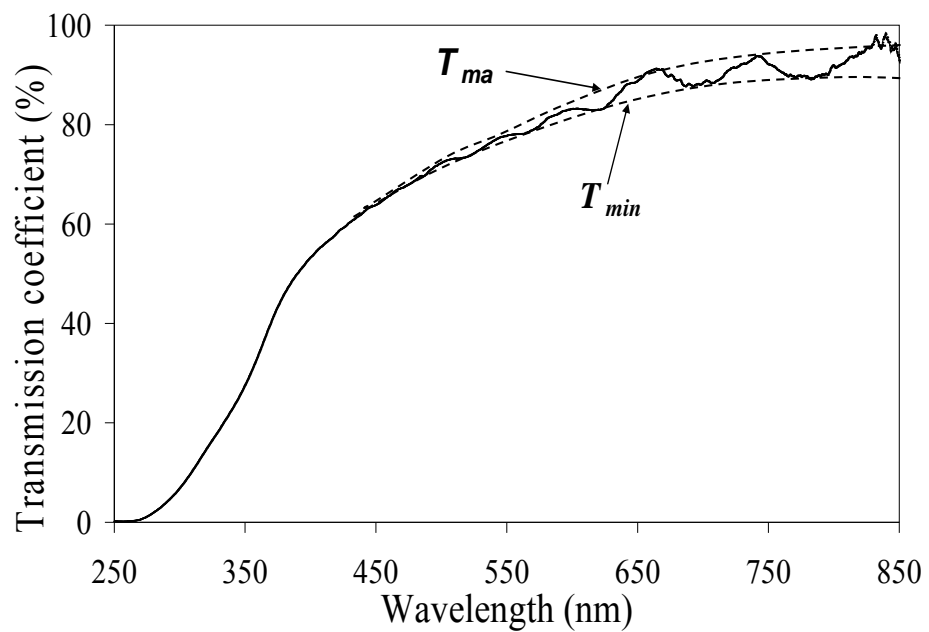
Figure 14 Room temperature dielectric constant and dissipation factor of $Ba(Zn_{1/3}Ta_{2/3})O_3$ film, inferred from measurements on interdigital structures. The film was grown from Zn-enriched target at 600 °C substrate temperature
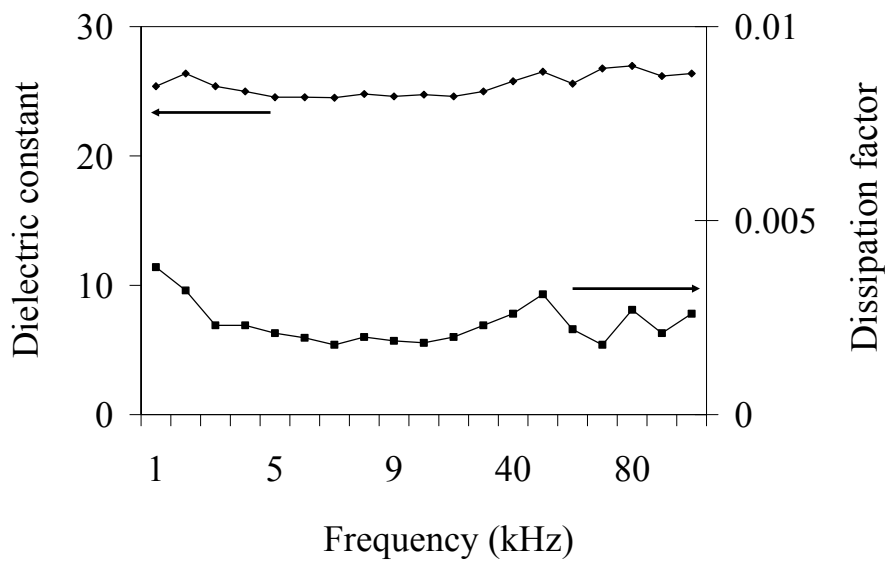
Figure 15. The temperature-dependence of the capacitance and dissipation factor of thin-film Ba(Zn$_{1/3}$Ta$_{2/3}$)O$_3$ interdigital capacitors. The results shown here are for a film grown at a 600 °C substrate temperature from an Zn-enriched target.
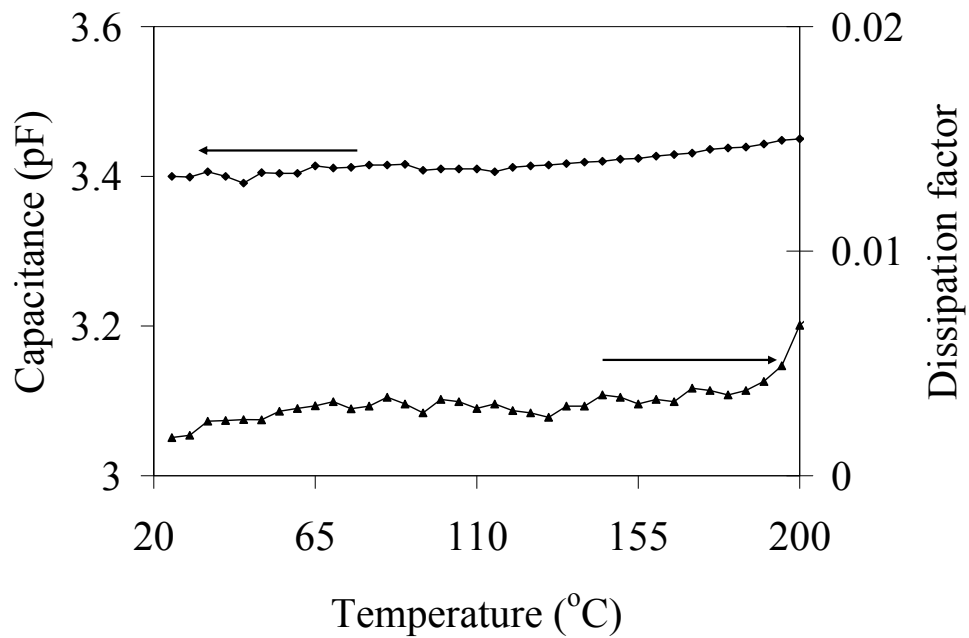
Figure 16. The influence of bias on the capacitance and dissipation factor of $Ba(Zn_{1/3}Ta_{2/3})O_3$ interdigital capacitors.
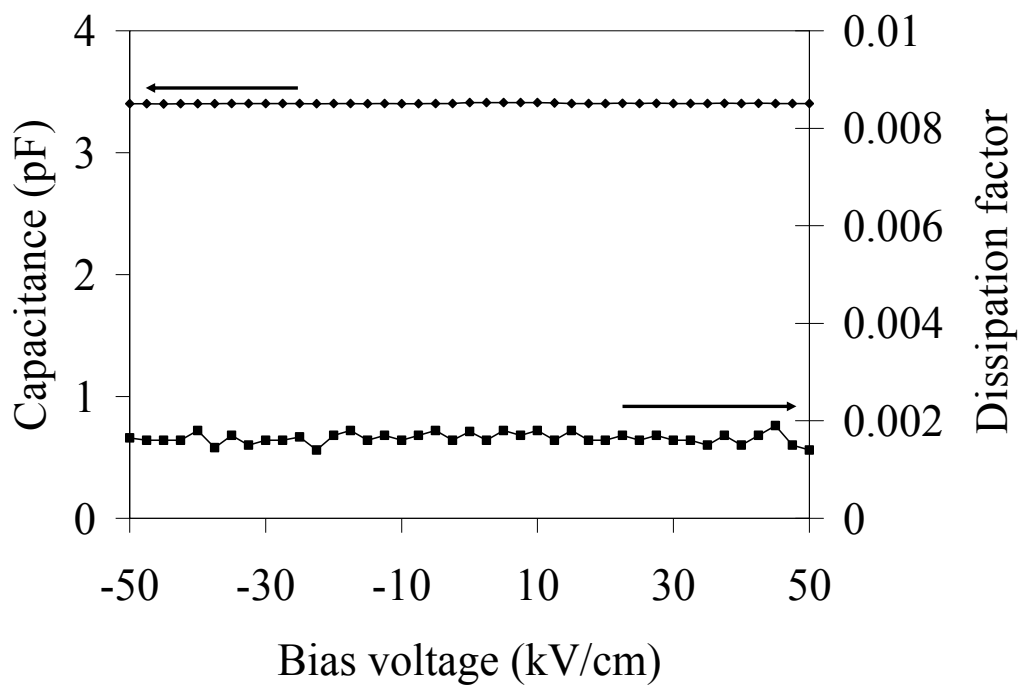
Figure 17. The leakage current of Ba(Zn$_{1/3}$Ta$_{2/3}$)O$_3$ thin films measured using an interdigital structure. The results shown here are for a film grown at a 600 °C substrate temperature from a Zn-enriched target.
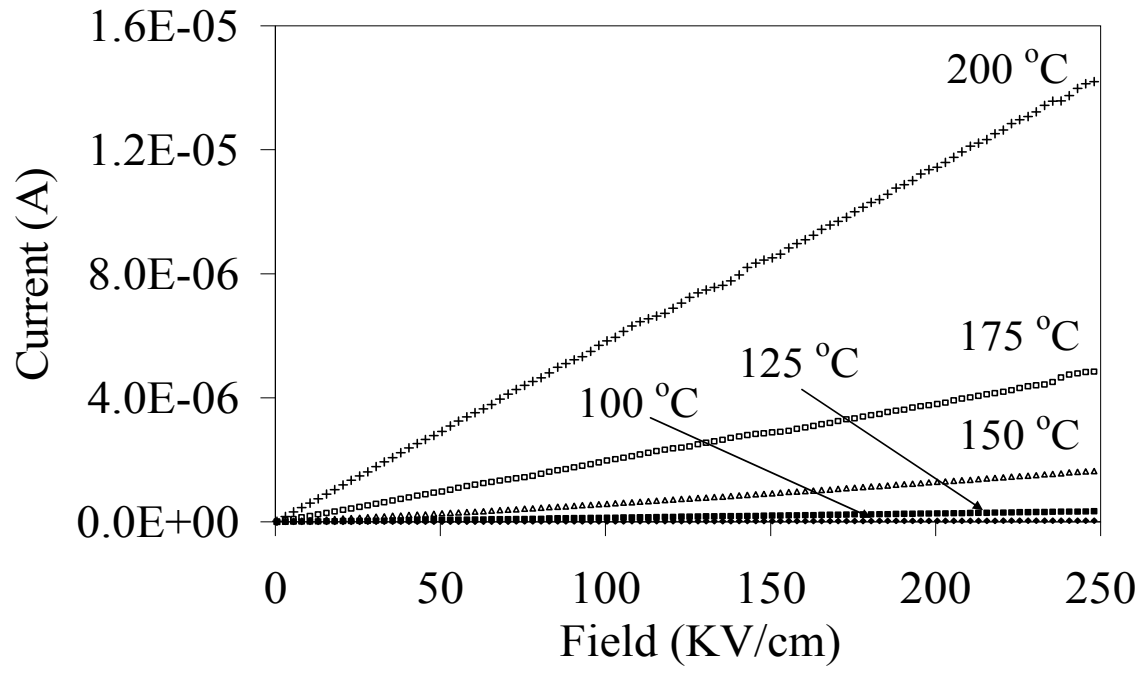
Figure 18. The Arrhenius plot of leakage current in the $Ba(Zn_{1/3}Ta_{2/3})O_3$ thin films grown from Zn-enriched target at 600 °C substrate temperature